

HEALTH AND MEDICINE

Uncovering temporospatial sensitive TBI targeting strategies via in vivo phage display

Briana I. Martinez^{1,2}, Gergey Alzaem Mousa¹, Kiera Fleck¹, Tara MacCulloch^{3,4}, Chris W. Diehnelt⁵, Nicholas Stephanopoulos^{3,4}, Sarah E. Stabenfeldt^{1*}

The heterogeneous pathophysiology of traumatic brain injury (TBI) is a barrier to advancing diagnostics and therapeutics, including targeted drug delivery. We used a unique discovery pipeline to identify novel targeting motifs that recognize specific temporal phases of TBI pathology. This pipeline combined in vivo biopanning with domain antibody (dAb) phage display, next-generation sequencing analysis, and peptide synthesis. We identified targeting motifs based on the complementarity-determining region 3 structure of dAbs for acute (1 day post-injury) and subacute (7 days post-injury) post-injury time points in a preclinical TBI model (controlled cortical impact). Bioreactivity and temporal sensitivity of the targeting motifs were validated via immunohistochemistry. Immunoprecipitation–mass spectrometry indicated that the acute TBI targeting motif recognized targets associated with metabolic and mitochondrial dysfunction, whereas the subacute TBI motif was largely associated with neurodegenerative processes. This pipeline successfully discovered temporally specific TBI targeting motif/epitope pairs that will serve as the foundation for the next-generation targeted TBI therapeutics and diagnostics.

INTRODUCTION

Traumatic brain injury (TBI) affects an estimated 1.7 million people in the United States each year and is a leading cause of death and disability for children and young adults in industrialized countries (1). Individuals who experience TBI are more likely to develop cognitive and behavioral deficits as well as physical conditions such as inhibited motor coordination and balance (2). These individuals are also more susceptible to acquiring neurodegenerative diseases than the non-injured population (3, 4). Treatment costs of TBI are estimated at \$76.5 billion annually in the United States alone (5), making TBI a great economic burden and public health concern.

TBI is characterized not by a singular event but a cascade of two separate injury phases. The initial insult disrupts the blood-brain barrier (BBB) and causes necrosis, tissue deformation, and cell shearing (6). This primary injury then catalyzes the secondary injury cascade, leading to an increase of inflammatory cytokines, mitochondrial damage, ischemia, and cell death (6). This pathology may persist for hours to months after the initial insult, introducing temporal complexity to the injured neural milieu (7). Unfortunately, the molecular and cellular mechanisms of injury progression are multifaceted and have yet to be fully elucidated. Consequently, this complexity affects the development of accurate diagnosis and treatment options.

The neurotrauma community has focused on TBI biomarker discovery largely for diagnostic and prognostic purposes. Biomarkers, objective signatures of injury or disease, can also inform and facilitate development of sensitive and specific therapeutic and diagnostic devices (8, 9), including the design of targeted therapeutic agents (10, 11). However, the temporal and dynamic evolution of TBI is a barrier to developing targeted therapeutics. Accordingly, the

identification and characterization of temporal TBI biomarkers and companion targeting strategies are critical for addressing current limitations in TBI treatment options.

Molecular-based biomarker discoveries are often driven by “top-down” approaches, where known molecular signal(s) or modulators are paramount to identifying candidate biomarkers. Recent TBI biomarker discoveries have capitalized on advances in neuroproteomics that use “bottom-up” approaches (12, 13). Several studies have successfully analyzed the proteome of the heterogeneous injury environment in preclinical TBI models to uncover hundreds of differentially expressed proteins that are candidate biomarkers of neural injury (12, 14). However, neuroproteomics approaches yield a large volume of data, leading to time-intensive analysis and difficulties translating biomarker candidates to the clinical space (12, 13). Moreover, such approaches only provide the molecular biomarker and not necessarily a complementary targeting motif for targeted therapeutic strategies.

Phage display, a powerful molecular screening technique to uncover molecular binding motifs, has revolutionized biomarker discovery in various cancers and, more recently, neurological conditions such as Alzheimer’s disease (AD) and stroke (15–18). This technique uses libraries of biological motif-displaying bacteriophages that are screened against a molecular target of interest. Bound bacteriophages are then collected and amplified to use in a subsequent biopanning round. This process is repeated to enrich the population of motifs that have strong affinity to the target of interest. Several phage display systems are available for use; the domain antibody fragment (dAb)–based display systems in particular hold distinct advantages (19, 20). These fragments represent the variable heavy (V_H) domain of a full-length antibody and contain three heavy complementarity-determining regions (HCDRs; 1, 2, and 3); HCDR3 specifically is the primary determinant of antigen binding specificity (21). The small molecular size of dAbs (12 to 15 kDa) makes them ideal for interacting with the neural milieu in vivo (22, 23). Here, we are the first reported group to leverage the advantages of dAb phage display to identify novel spatiotemporal targeting motifs for TBI.

¹School of Biological and Health Systems Engineering, Arizona State University, Tempe, AZ, USA. ²School of Life Sciences, Arizona State University, Tempe, AZ, USA. ³School of Molecular Sciences, Arizona State University, Tempe, AZ, USA. ⁴Biodesign Institute Center for Molecular Design and Biomimetics, Arizona State University, Tempe, AZ, USA. ⁵Biodesign Institute Center for Innovations in Medicine, Arizona State University, Tempe, AZ, USA.

*Corresponding author. Email: sarah.stabenfeldt@asu.edu

Using an antibody fragment as the discovery platform in combination with next-generation sequencing (NGS) enables a multitude of options for generating subsequent targeting motifs (24). The traditional approach of conducting NGS bioinformatics analysis of phage biopanning rounds followed by recombinant protein production to generate reproducible antibody fragments (24) is time consuming and notoriously fraught with protein stability and affinity tag degradation issues (25). To address these limitations, “synthetic antibody”-type constructs have been investigated with particular focus on the HCDR3 region due to the dominant role in antigen recognition and specificity (26–28). Previously reported HCDR3 constructs mimic the binding specificity and capacity of full-length antibodies for factors such as platelet aggregation and HIV-1 promoter at a fraction of the size (27, 28). Moreover, HCDR3 constructs have been immobilized on the surface of nanoparticles to generate nanoparticles with high specificity and affinity to the target of interest (26).

Here, we present the findings from our innovative discovery pipeline that involved *in vivo* phage display biopanning, NGS bioinformatics analysis, HCDR3 peptide construct development, and subsequent proteomic analysis that ultimately identified novel spatiotemporal TBI targeting motifs and characterized the heterogeneous injury milieu. Specifically, we report two HCDR3 constructs that target injured brain tissue with high specificity acutely (1 day) or subacutely (7 days) post-injury in a preclinical TBI model [mouse controlled cortical impact (CCI) model]. A constrained peptide loop biochemistry technique in combination with NGS bioinformatics

of dAb phage biopanning populations enabled generation of novel HCDR3 constructs. These HCDR3 constructs demonstrated spatio-temporal specificity for either acute or subacute TBI as validated via immunohistochemistry (IHC). Immunoprecipitation–mass spectrometry (IP-MS) with the HCDR3 constructs identified several potential targets associated with metabolic dysfunction and neurodegenerative processes expressed at the acute and subacute time points, respectively. Collectively, these findings lay the foundation for novel TBI targeting therapeutic and diagnostic strategies.

RESULTS

dAb phages bind to injured brain tissue *in vivo*

A dAb phage library was intravenously injected into CCI injured mice at 1, 7, and 21 days post-injury (dpi) (Fig. 1). Phage accumulation was analyzed through titer analysis to confirm that the phage library was given sufficient time to bind to target tissues. Titers determined that phage accumulated in all extracted tissues, with the spleen having the highest total colony-forming units (CFU) per gram tissue of 1.05×10^7 (table S1). Up to 1.21×10^6 CFU/g tissue were recovered from neural tissue of each cohort through trypsinization, including sham controls. The percentage of recovered phage from the ipsilateral hemisphere increased from biopanning round 1 to round 2 for both the acute and subacute time points (increased 28 and 37%, respectively), indicating successful enrichment of affinity binders to target tissue (fig. S1, B and C). The percent of CFU bound to chronic injured and sham tissue were similar between biopanning rounds (fig. S1, A and D).

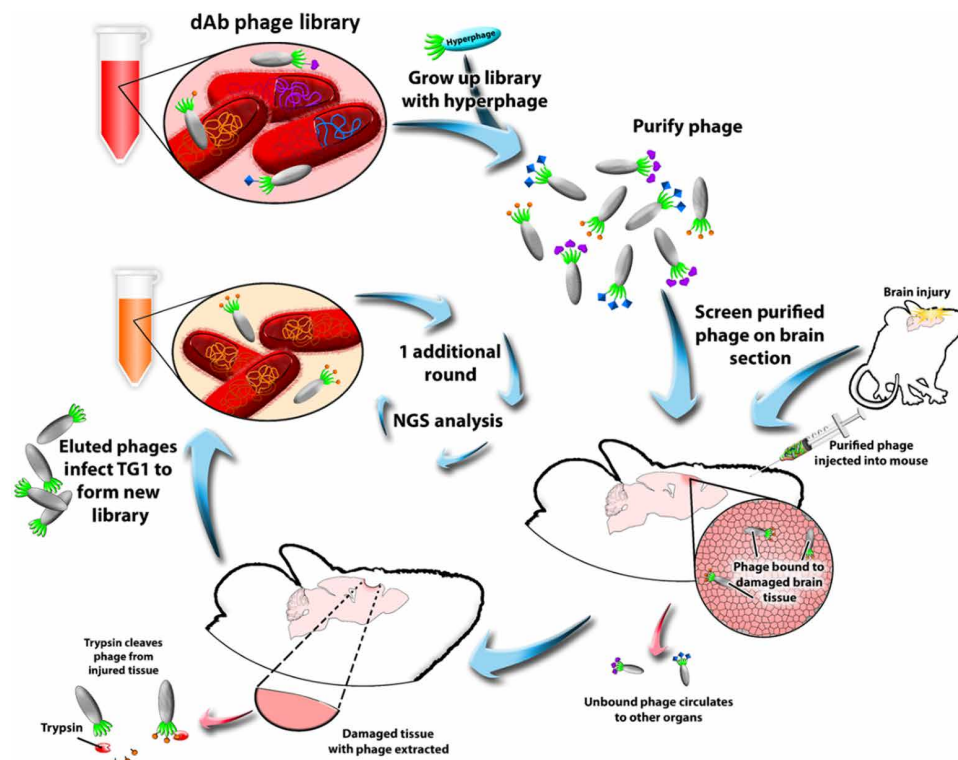


Fig. 1. Schematic of phage display biopanning. A dAb phage parent library was produced and purified and then intravenously injected into a mouse that sustained a controlled cortical impact (CCI) at a distinct time point (1, 7, or 21 dpi) or a sham injury (sacrificed 1 day post-procedure). Tissues were extracted, lysed, and trypsinized to cleave phage from tissue. The phage library from the ipsilateral hemisphere was then amplified with TG1 *E. coli* and applied in the final round of biopanning. Recovered phages were then analyzed using NGS.

NGS analysis reveals HCDR3 sequences specific to distinct injury time points

dAb phage libraries were sequenced via NGS; subsequent analyses focused on the HCDR3 sequence. This region is the only HCDR within the dAb structure that differs in canonical composition and residue length, indicating that these characteristics promote unique antigen binding specificity (29). Injury libraries yielded thousands of HCDR3s for each biopanning round, with between 200,000 and 600,000 sequences in the final biopanning round (Fig. 2A). Bioinformatics analysis comparing the HCDR3 populations illustrated that only a small fraction of HCDR3 sequences were similar across time points post-injury, suggesting that dAb phage interacted uniquely with the neural microenvironment depending on the temporal condition. After the final biopanning round, less than 20% of HCDR3 sequences from each injury time point population were identical to the control propagation library, suggesting that injury-enriched populations were specific to neural injury pathology (Fig. 2B).

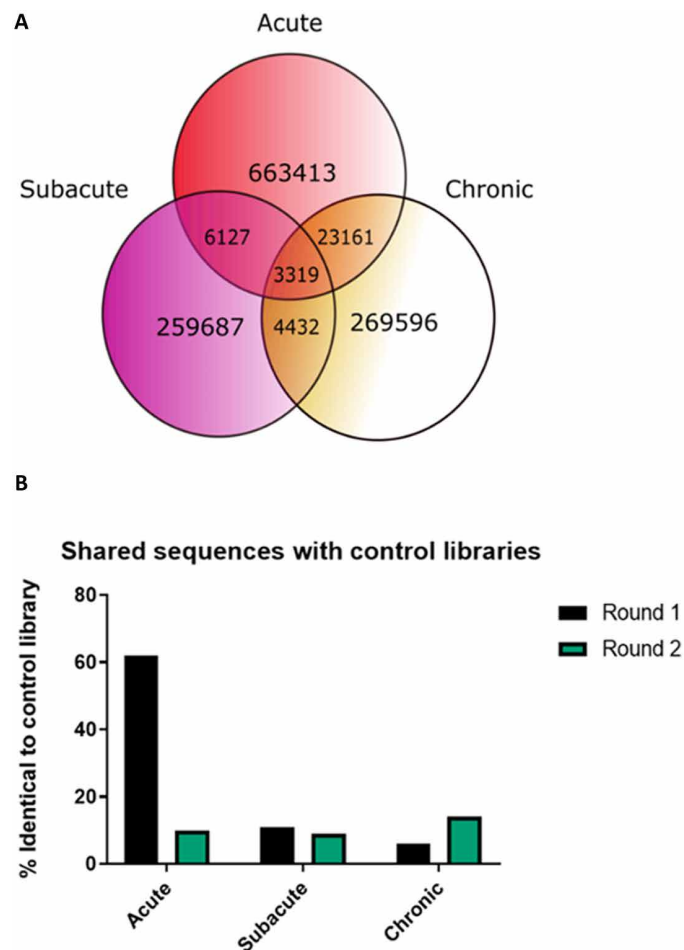


Fig. 2. Sequence population diversity. (A) Comparison of recovered HCDR3s across injury time points represented by a Venn diagram. A majority of the recovered sequences were unique to their distinct time point, while a small fraction was found in multiple injury libraries simultaneously. (B) Comparison of recovered injury library HCDR3s against control propagation library. For the acute injury library, the percentage of sequences found in the control propagation library drastically decreased after biopanning. Both the subacute and chronic injury libraries yielded less than 20% similarity with controls across biopanning rounds.

Biopanning increases frequency of neural injury-specific HCDR3s

Across all conditions, phage populations recovered from the ipsilateral hemisphere in the second biopanning round yielded substantially more sequences with higher frequency of expression (>200 reads) than the first round (fig. S2). This shift in frequency is representative of the biopanning process enriching the population of sequences that have preferential binding to injured neural tissue. Sequences that had an increased frequency in the final biopanning round than the first were categorized as “enriched” (Fig. 3). Only 6.7 and 3.0% of sequences met this criterion for the acute and subacute libraries, respectively, which provided an opportunity to identify HCDR3s that were highly expressed due to affinity selection (table S2).

Phage display-derived HCDR3s are temporally specific to distinct injury time points

A heatmap of normalized sequence reads per million (RPMs) was constructed to visualize temporal relationships of the enriched HCDR3s for each time point. A multitude of sequences with the highest RPMs in their respective groups were observed in other time points post-injury (Fig. 4A). For example, several HCDR3s in the acute time point were also highly represented in the subacute and chronic time points. While this finding may indicate commonalities in pathology across time points, we aimed to identify temporally

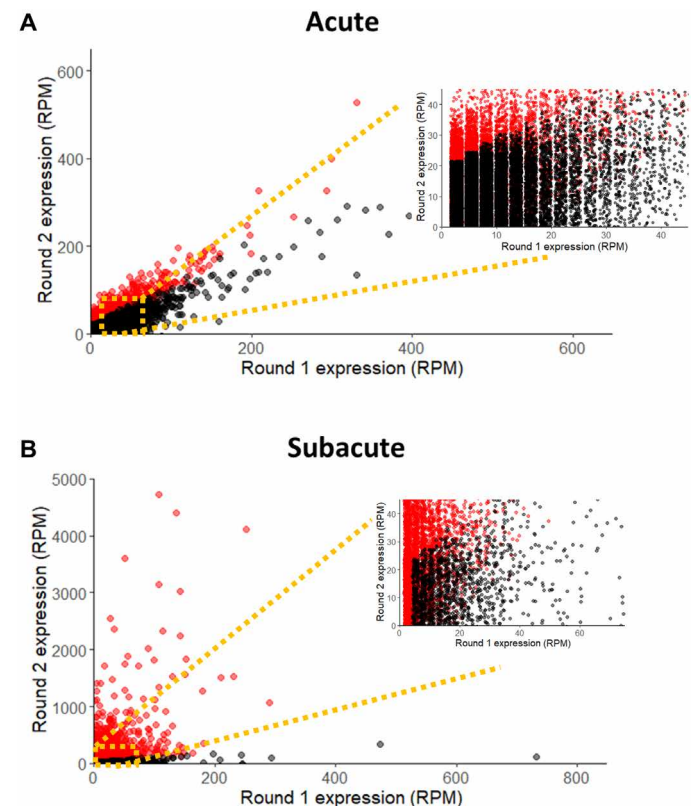


Fig. 3. RPM of sequences increased after biopanning. Relationship between individual sequence RPMs after the biopanning rounds is visualized with scatterplots for (A) acute and (B) subacute injury libraries. Black data points represent sequences that were not enriched through biopanning. Red data points represent sequences that were enriched through biopanning. Insets highlight density of sequences within the low expression range.

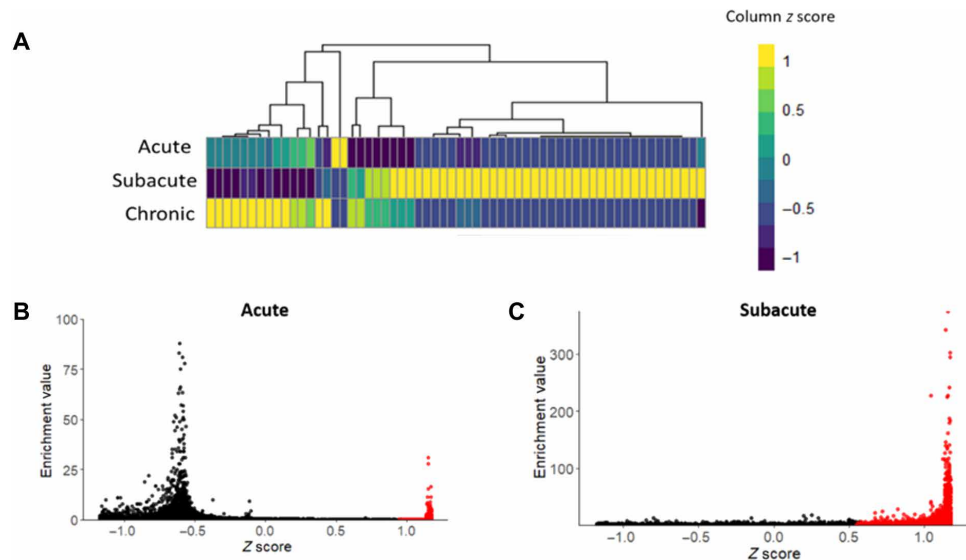


Fig. 4. Analysis of HCDR3 temporal specificity. (A) Representative heatmap of the top 20 highest-frequency HCDR3s identified in each injury time point and their expression in adjacent time points. Z scores were calculated by column (individual sequences). (B and C) Scatterplots were generated to visualize the relationship between enrichment value (defined as round 2 reads/round 1 reads) and z score (B) acute and (C) subacute injury HCDR3s. Black data points represent sequences that did not meet z-score threshold criteria. Red data points represent sequences that met z-score threshold criteria. Z score of 1 = high specificity, z score of -1 = low specificity.

sensitive and specific HCDR3 sequences. Therefore, creating a z-score matrix of the sequences provided an opportunity to develop stringent criteria for selecting time point–specific sequences for HCDR3 construct design. Z scores were averaged for each time point and used as a threshold to identify HCDR3s with strong specificity for their distinct time point. Of the enriched sequences for both time points, less than 2% met z-score criteria (Fig. 4, B and C, and table S2). This bioinformatics analysis narrowed the pool of candidate biological motifs to an exclusive and focused group. For final selection, HCDR3s were required to (i) be unique to a distinct temporal phase post-injury, as determined by z-score normalization and comparison against other injury libraries, (ii) be enriched after biopanning, and (iii) not be present in control libraries (i.e., propagation or peripheral organs). On the basis of these guidelines, two HCDR3s were selected for each injury time point: one sequence with the highest frequency and another with the highest fold enrichment value (Table 1). These HCDR3 sequences served as the template to generate biotinylated cyclized HCDR3 constructs in an effort to maintain three-dimensional confirmation of the native HCDR3 loop (Fig. 5). The HCDR3 constructs were synthesized and purified via high-performance liquid chromatography (HPLC), validated by matrix-assisted laser desorption/ionization (MALDI) MS (fig. S5).

Validation of spatiotemporal affinity

IHC assessed the specificity of HCDR3 constructs to CCI injury sections collected at the three different phases post-injury (acute = 1 dpi, subacute = 7 dpi, chronic = 21 dpi, and sham non-injured tissue). IHC with the high-frequency acute-1 construct (A1) yielded no detectable signal on acute injury tissue (fig. S3). The highly enriched acute-2 construct (A2) exhibited significant bioreactivity determined by the area of positive fluorescence on 1-dpi tissue (Fig. 6A) compared to sham tissue (Fig. 6B) ($n = 6$ per group, $P = 0.0120$) and 7-dpi tissue ($n = 5$, $P = 0.0221$) (Fig. 6, C and D). While trending toward significance, no statistically significant differences were

observed between 1- and 21-dpi tissue ($n = 4$ to 6 per group, $P = 0.0658$) (Fig. 6D). Positive stain with the high-frequency subacute-1 construct (SA1) was observed in the peri-injury region of the 7-dpi tissue, while this localization was not observed in sham brain sections ($n = 5$ to 6 per group, $P = 0.0079$) (Fig. 6E). No detectable signal was observed with high enrichment subacute-2 construct (SA2). A trend for SA1 specificity to the 7-dpi tissue was noted compared to 1- and 21-dpi tissue, albeit not statistically significant ($n = 4$ to 6 per group, $P = 0.0993$ and $P = 0.0780$, respectively). No sex-dependent differences were observed within or between injury groups. Control HCDR3 constructs (derived from spleen, heart, and propagation phage library; table S3) showed no detectable signal on injured tissue at 1 or 7 dpi, demonstrating that the positive signal we observed from A2 and SA1 were not due to nonspecific artifact derived from the construct structure (fig. S4).

IP-MS isolates proteins involved in neurodegenerative and microtubule-based processes

IP-MS analysis identified 17 and 64 proteins specific to the injury condition when using A2 and SA1 as capture motifs, respectively [false discovery rate (FDR) < 0.01] (tables S4 and S5). For the acute injury phase, Na^+/K^+ -transporting adenosine triphosphatase (ATPase) subunit α and calcium/calmodulin-dependent protein kinase II subunit α were among the top represented proteins isolated by A2 based on the number of peptides identified from the LC-MS data. In the subacute phase, heat shock cognate 71 kDa and heavy polypeptide neurofilament were the top represented proteins isolated by SA1 (Table 2). Functional cluster analysis of candidate proteins revealed two annotation clusters from A2-isolated proteins and eight from SA1-isolated proteins (Tables 3 and 4). For A2, several biological processes and molecular functions in annotation cluster 1 were similarly represented across groups, such as microtubule-based processes and guanosine triphosphatase (GTPase) activity [Benjamini-Hochberg (BH)-adjusted $P < 0.001$]. SA1 annotation cluster 2 revealed

Table 1. Selected HCDR3s.

	Enrichment value	Frequency	Z score	Sequence
A1	2.47	111	1.154	TAERDARTFQY
A2	22	22	1.155	SLYGSSRHTAPISF
SA1	49	638	1.155	TDLAVAHPVRY
SA2	17.57	246	1.148	AAPSWNNHVSY

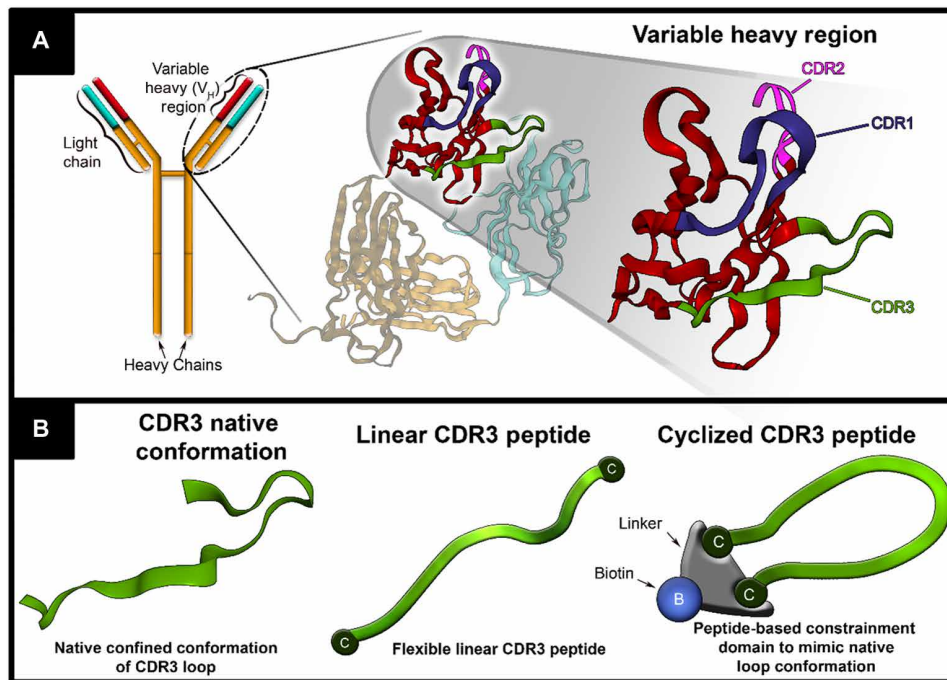


Fig. 5. Cyclized HCDR3 peptides. (A) Representation of HCDRs. dAbs consist of the variable heavy region of a full-length antibody. Each dAb contains three HCDRs, with HCDR3 facilitating antigen binding. (B) Representation of a cyclized HCDR3 peptide. Each HCDR3 peptide construct is conjugated to a bivalent peptide linker that contained a C-terminal biotin.

amyotrophic lateral sclerosis (ALS) as notable pathway (BH-adjusted $P = 0.12$) alongside proteins involved in processes such as axon development (BH-adjusted $P = 0.0010$) and microtubule cytoskeleton organization (BH-adjusted $P = 0.0072$). SA1 annotation cluster 5 contained several neurodegenerative processes, such as Huntington's disease (HD) (BH-adjusted $P = 0.02$), AD (BH-adjusted $P = 0.05$), and Parkinson's disease (PD) (BH-adjusted $P = 0.58$).

DISCUSSION

Diagnosis and treatment of TBI is confounded by the temporal and spatial complexity of pathological progression. Analysis of temporal biomolecular mechanisms provides insight into injury progression that may better inform the development of therapeutic and diagnostic tools. In this study, we leveraged the power of unbiased phage display to identify and develop novel biomolecular motifs that specifically recognize elements of acute and subacute TBI pathology. In vivo phage biopanning was conducted in a CCI rodent model at three distinct time points following injury (1, 7, and 21 dpi) to perform a robust bioinformatics-driven assessment of enriched phage

populations for each time point. The spatiotemporal specificity of HCDR3 constructs based on the NGS data was validated first with IHC analysis, demonstrating the strength of this high-throughput screening and sequencing methodology. Using IP-MS, we positively identified several candidate proteins as potential targets for acute (A2) and subacute (SA1) targeting motifs, respectively. The elegance of phage-based approach, in contrast to traditional neuroproteomics [i.e., whole brain tissue analysis to identify differentially expressed proteins via MS (12)], is that phage biopanning leverages molecular evolution to narrow the molecular pool for biomarker candidate selection.

dAb libraries are advantageous to screening against neural tissue in vivo due to their small size (12 to 15 kDa), high affinity, and ability to effectively bind to brain vasculature under normal BBB conditions (23, 30). dAb phage accumulation in naïve and chronic injury neural tissue was comparable across biopanning rounds, while accumulation within acute and subacute injury groups drastically increased from biopanning round 1 to round 2. While phage displayed motifs can target brain vasculature, in vivo screening in models of injury and degeneration has demonstrated that BBB disruption

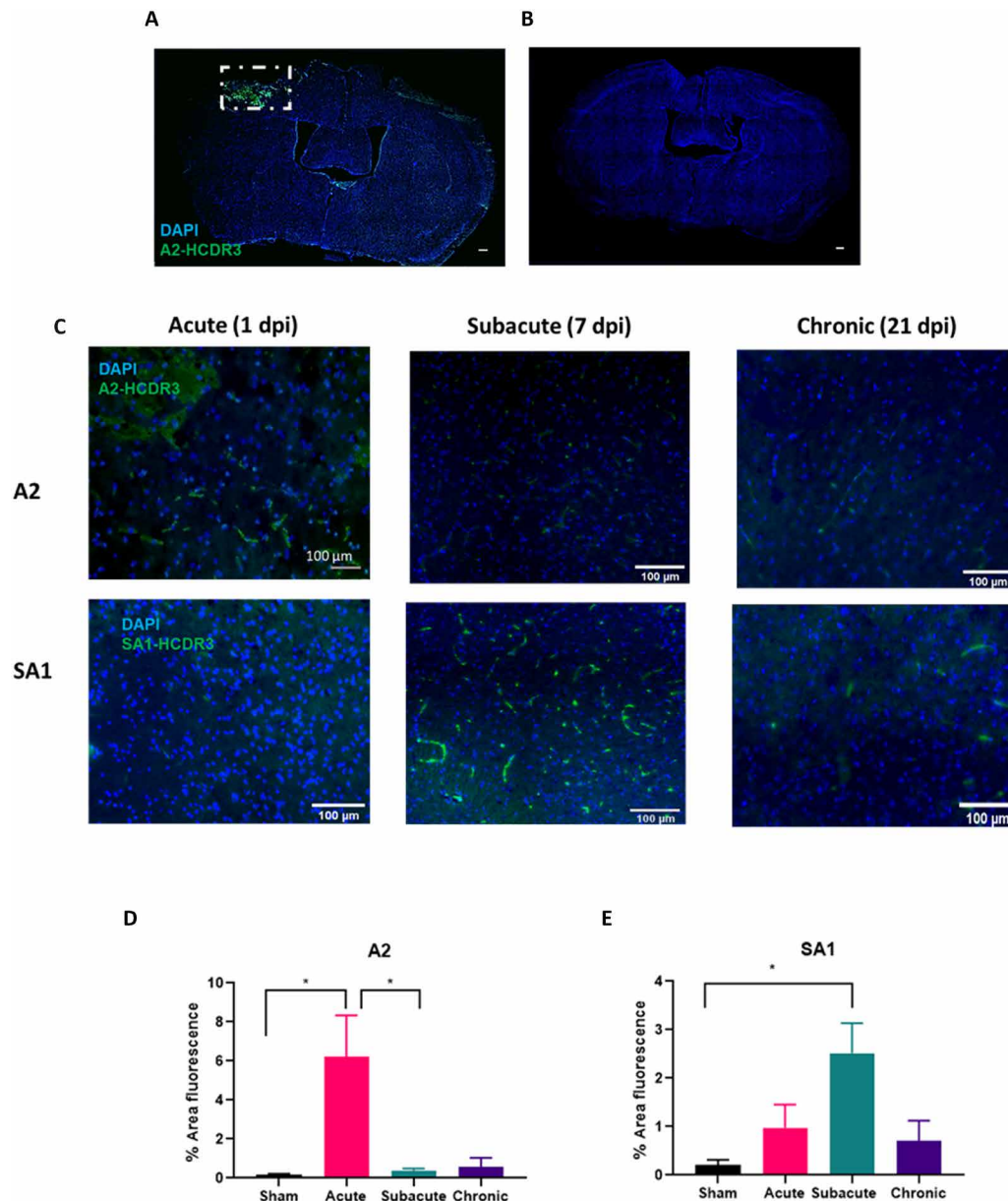


Fig. 6. HCDR3 constructs show selectivity to injured tissue. (A) Qualitative representation of A2 acute injury-specific HCDR3 (green) and cell nuclei (blue) in 1-dpi tissue. Region of interest (ROI) represented in white box. Scale bars, 200 μm . (B) Magnification ($\times 5$) of A2 construct staining on sham tissue. Scale bars, 200 μm . (C) Panel of A2 and SA1 staining on acute (1 dpi), subacute (7 dpi), and chronic (21 dpi) tissue. Scale bars, 100 μm . Quantification of % area fluorescence in 1500 $\mu\text{m} \times 1500 \mu\text{m}$ ROI ($n = 5$ to 6 biological replicates per group) for A2 (D) and SA1 (E). Data expressed in mean + SEM. * $P < 0.05$.

provides opportunity for extravascular binding of the phage (31). Notably, the disrupted state of the BBB persists in the CCI model up to 7 dpi, allowing macromolecules and potential therapeutic agents to gain extravascular access via intravenous circulation (32, 33). The compromised condition of the BBB may have permitted intravenously injected phage to access extravascular targets at the acute and subacute time points; our data corroborate this phenomenon whereby relatively lower percentage of phage accumulated in sham and chronic injury cohorts (fig. S1) (17).

Recent sequencing advances in NGS capabilities are instrumental to the identification of candidate biological motifs in phage display libraries. NGS analysis provides an opportunity to uncover the entire

population of phage display libraries at a sequencing space of 10^5 to 10^7 , in comparison to 20 to 100 for traditional Sanger sequencing methods (34). This NGS analysis also minimizes the probability of selecting false-positive clones that may be overrepresented in the library due to propagation advantages, amplified as a consequence of repetitive screening (35). Applying NGS analysis to the screening results circumvented this dilemma by providing a platform to achieve a thorough analysis with only two biopanning rounds. Both advantages are critical for the analysis of a library derived from in vivo biopanning of the neural injury microenvironment.

In lieu of recombinant protein production, we addressed the challenge of bioreactivity validation by designing novel peptide-based

Table 2. Candidate proteins isolated by A2 and SA1.

Targeting construct	Accession ID	Description	No. of peptides
A2	Q8VDN2	Sodium/potassium-transporting ATPase subunit α -1	12
	P11798-1	Calcium/calmodulin-dependent protein kinase type II subunit α	9
	Q6IFX2	Keratin type I cytoskeletal	4
	P50446	Keratin 6A	38
	P63017	Heat shock cognate 71 kDa protein	32
	P19246	Neurofilament, heavy polypeptide	24
	P20029	ER chaperone BiP	18
	P62204	Calmodulin 1	13
	O08553	Dihydropyrimidinase-like 2	12
	P12367	Protein kinase, cAMP-dependent regulatory, type II α	12
	P68254-1	14-3-3 protein θ	12
	Q3TTY5	Keratin 2	6
	P70670	Nascent polypeptide-associated complex α polypeptide	6
	P57776-1	Elongation factor 1- δ	6
	SA1	P80316	Chaperonin containing Tcp1, subunit 5 (ϵ)
Q9DB20		ATP synthase, H ⁺ transporting, mitochondrial F1 complex, O subunit	4
P42932		Chaperonin containing Tcp1, subunit 8 (θ)	4
Q8VEK3		Heterogeneous nuclear ribonucleoprotein U	3
P12970		Ribosomal protein L7A	3
P62918		Ribosomal protein L8	2
P07356		Annexin A2	3
Q923G2		Polymerase (RNA) II (DNA directed) polypeptide H	3
P84089		Enhancer of rudimentary homolog	3
P62754		Ribosomal protein S6	2
P97350		Plakophilin 1	2
P10639		Thioredoxin 1	2

HCDR3 constructs that mimic the constrained HCDR3 loop structure, motivated by prior studies (21), thereby enabling high-throughput production via direct peptide synthesis and facile biochemical modifications to fabricate the constrained cyclic HCDR3 loop structure. The HCDR3 has been identified as the main contributor to binding specificity of antibodies and truncated antibody fragments. Prior studies have highlighted the utility of generating HCDR3 peptide variants as a synthetic antibody with comparable binding efficiency to full-length antibodies (36). Our data further support this reductionist approach, and future studies will focus on potential mechanisms and molecular tuning to optimize the HCDR3 loop structure.

Our validation results readily demonstrated the critical need for thorough testing of each phage identified candidate motif. For example, A1 was identified on the basis of our selection criteria for the

acute time point based on the high frequency in biopanning round 2 population, yet IHC assessment did not reveal detectable bioreactivity with fixed mouse brain tissue at 1 dpi. In contrast, A2, selected namely for the high fold enrichment value from biopanning round 1 to round 2, exhibited high sensitivity and affinity to the peri-injury region at 1 dpi. For the subacute constructs, the opposite effect was observed with constructs targeting subacute injury, with SA1, a construct selected for its high frequency, positively binding to injured neural tissue. A1 had the highest observed frequency for its time point, yet it only exhibited a fold enrichment value of 2.47, much lower than A2's enrichment value of 22. Furthermore, SA2's enrichment value of 17.57 dwarfed in comparison to SA1's value of 49 (Table 1). These results may suggest that enrichment in biopanning plays a critical role in selecting/identifying high-affinity HCDR3s. However,

Table 3. DAVID functional annotation clustering of A2 proteins.

Category	Term	Count	P	Benjamini
Annotation cluster 1—Enrichment score: 3.4				
GOTERM_BP_DIRECT	Microtubule-based process	4	1.80E−06	1.80E−04
KEGG_PATHWAY	Gap junction	4	2.60E−05	6.60E−04
KEGG_PATHWAY	Phagosome	4	2.10E−04	2.60E−03
GOTERM_MF_DIRECT	GTPase activity	4	4.40E−04	1.10E−02
GOTERM_CC_DIRECT	Microtubule	4	1.20E−03	1.90E−02
GOTERM_MF_DIRECT	GTP binding	4	2.50E−03	3.40E−02
GOTERM_CC_DIRECT	Cytoskeleton	5	4.80E−03	6.70E−02
GOTERM_MF_DIRECT	Nucleotide binding	6	1.00E−02	1.10E−01
GOTERM_CC_DIRECT	Nucleus	5	6.00E−01	1.00E+00
Annotation cluster 2—Enrichment score: 0.66				
GOTERM_MF_DIRECT	Protein binding	7	6.10E−02	3.70E−01
GOTERM_CC_DIRECT	Protein complex	3	6.30E−02	5.20E−01
GOTERM_CC_DIRECT	Plasma membrane	4	6.60E−01	1.00E+00
GOTERM_CC_DIRECT	Membrane	4	9.00E−01	1.00E+00

further testing is required to fully elucidate the factors that influence bioreactivity of phage-selected HCDR3s.

The CCI mouse model is a well-established and characterized model that has been assessed at different phases of injury (6). A2 positive staining on 1-dpi tissue indicated significant bioreactivity compared to sham and subacute tissue, with a concentrated visual appearance restricted to the injury penumbra. In comparison, SA1 positive staining on 7-dpi tissue was punctate and more dispersed, consequently yielding a lower average fluorescence per area than the acute group. While A2 demonstrated nearly exclusive bioreactivity to acute injury (1 dpi), SA1 IHC staining exhibited a gradual trend in bioreactivity across 1, 7, and 21 dpi, although bioinformatics analysis suggested that this construct was uniquely specific to subacute injury phase. Positive staining on 7 dpi was statistically significant in comparison to the sham cohort accompanied by a notable increase observed on 1 dpi tissue peaking at 7 dpi and then tapering at 21 dpi. This observed pattern may suggest that the SA1 target is a protein that is expressed early in the secondary injury phase and becomes more prominent as the cascade continues, such as a protein that contributes to glial injury, apoptosis, or neuroinflammation (13).

Further characterization of our HCDR3 constructs was performed by IP-MS analysis. Proteins that were identified in more than one biological replicate sample were subjected to Database for Annotation, Visualization, and Integrated Discovery (DAVID) functional annotation analysis to provide an overview of gene ontology annotation terms associated with proteins of interest (Tables 3 and 4). For both the A2 and SA1 constructs, GTPase activity and microtubule-associated processes were one of the notable pathways identified in DAVID functional annotation analysis. GTPases of different families have various associations with apoptosis and regeneration (37, 38). Microtubule-associated processes were also identified as a significant process shared between A2- and SA1-isolated proteins. Microtubule dysfunction is implicated in axonal degeneration after injury and may contribute to tau-related pathologies (39).

Neurodegenerative pathways such as AD, PD, and ALS were only identified in the SA1 group and not in the A2 group (Table 3). There is evidence that individuals with TBI are more at risk for ALS than non-injured individuals, but the mechanisms of this association are yet to be determined (40). TBI may also be a risk factor for both AD and PD because of the protein misfolding and degeneration involved in chronic pathology (41, 42).

To identify candidate proteins for each of the targeting constructs, IP-MS-identified proteins that were found in more than one biological replicate and were unique to a distinct injury time point were considered along with their peptide matches. For the A2 targeting construct, Na⁺/K⁺ ATPase was determined to be a potential candidate due to its specificity to the injury time point and its high number of peptide matches relative to the other identified proteins in the targeting group (12 peptides; Table 2). Na⁺/K⁺ ATPase is currently being explored as a therapeutic target to mitigate the effects of ischemic stroke, as its increase is found to be neuroprotective in slice cultures (43). Calcium/calmodulin-dependent protein kinase type II subunit α (α -CaMKII) was also among the A2-isolated proteins with the highest number of peptides (nine peptides; Table 2). This synaptic plasticity-related protein is reported with increased activation in rat hippocampus and parietal cortex tissues in acute TBI time points (44). In rat hippocampal slice cultures, α -CaMKII was also found to be a key component in the oxidative stress response after hypoxic ischemia (45).

SA1-isolated proteins strongly associated with neurodegenerative processes such as HD, AD, and PD. Heat shock cognate 71 kDa and endoplasmic reticulum (ER) chaperone BiP (32 and 18 peptides; Table 2), members of the heat shock protein 70 family, have both been identified as components of PD and the apoptosis signaling pathway (46, 47). ER chaperone BiP, a monitor of ER stress, is induced in AD in response to protein misfolding and cell death (48, 49). In addition, a reduction in ER chaperone BiP expression leads to the acceleration of prion disease pathology (50). Comparatively, an increase in ER chaperone BiP expression is suggested to

Table 4. DAVID functional annotation clustering of SA1 proteins.

Category	Term	Count	P	Benjamini
Annotation cluster 1—Enrichment score: 6.29				
GOTERM_MF_DIRECT	Structural constituent of cytoskeleton	10	4.00E-12	7.30E-10
GOTERM_BP_DIRECT	Microtubule-based process	7	2.50E-09	5.50E-07
GOTERM_CC_DIRECT	Microtubule	12	2.60E-09	1.30E-07
GOTERM_CC_DIRECT	Cytoskeleton	15	3.10E-06	5.10E-05
KEGG_PATHWAY	Gap junction	7	3.40E-06	2.50E-04
GOTERM_MF_DIRECT	GTPase activity	7	6.60E-05	1.50E-03
KEGG_PATHWAY	Phagosome	7	1.70E-04	3.40E-03
GOTERM_MF_DIRECT	GTP binding	7	1.70E-03	1.90E-02
Annotation cluster 2—Enrichment score: 4.22				
GOTERM_BP_DIRECT	Intermediate filament bundle assembly	5	1.10E-09	5.10E-07
GOTERM_CC_DIRECT	Neurofilament	4	2.00E-06	4.00E-05
GOTERM_BP_DIRECT	Neurofilament cytoskeleton Organization	4	3.10E-06	2.40E-04
GOTERM_BP_DIRECT	Neurofilament bundle assembly	3	2.70E-05	1.50E-03
GOTERM_BP_DIRECT	Microtubule cytoskeleton organization	5	2.10E-04	7.20E-03
GOTERM_BP_DIRECT	Axon development	3	3.20E-04	1.00E-02
GOTERM_BP_DIRECT	Intermediate filament cytoskeleton organization	3	1.10E-03	2.80E-02
KEGG_PATHWAY	ALS	3	2.60E-02	1.20E-01
GOTERM_MF_DIRECT	Protein heterodimerization activity	6	2.80E-02	2.00E-01
Annotation cluster 3—Enrichment score: 3.06				
GOTERM_CC_DIRECT	Extracellular vesicle	7	6.40E-09	2.50E-07
GOTERM_BP_DIRECT	Sodium ion export from cell	4	2.20E-06	2.40E-04
GOTERM_CC_DIRECT	Sodium:potassium-exchanging ATPase complex	4	2.90E-06	5.10E-05
GOTERM_BP_DIRECT	ATP hydrolysis-coupled proton transport	5	2.90E-06	2.40E-04
KEGG_PATHWAY	Endocrine and other factor-regulated calcium reabsorption	6	4.90E-06	2.50E-04
GOTERM_MF_DIRECT	Sodium:potassium-exchanging ATPase activity	4	5.60E-06	2.10E-04
GOTERM_BP_DIRECT	Cellular potassium ion homeostasis	4	5.70E-06	3.70E-04
KEGG_PATHWAY	Gastric acid secretion	6	2.50E-05	8.30E-04
GOTERM_BP_DIRECT	Cellular sodium ion homeostasis	4	2.90E-05	1.50E-03
GOTERM_BP_DIRECT	Potassium ion import	4	6.60E-05	2.70E-03
KEGG_PATHWAY	Proximal tubule bicarbonate reclamation	4	1.60E-04	3.40E-03
KEGG_PATHWAY	Thyroid hormone synthesis	5	3.70E-04	6.20E-03
GOTERM_CC_DIRECT	Sarcolemma	5	4.10E-04	3.70E-03
GOTERM_CC_DIRECT	Intercalated disc	4	4.60E-04	3.90E-03

continued on next page

Category	Term	Count	P	Benjamini
KEGG_PATHWAY	Salivary secretion	5	5.30E-04	7.60E-03
KEGG_PATHWAY	Adrenergic signaling in cardiomyocytes	6	6.10E-04	7.80E-03
KEGG_PATHWAY	Insulin secretion	5	8.10E-04	8.90E-03
KEGG_PATHWAY	Mineral absorption	4	9.00E-04	8.90E-03
KEGG_PATHWAY	Aldosterone-regulated sodium reabsorption	4	9.70E-04	8.90E-03
GOTERM_MF_DIRECT	Potassium ion binding	3	1.10E-03	1.60E-02
KEGG_PATHWAY	Carbohydrate digestion and absorption	4	1.10E-03	9.40E-03
GOTERM_MF_DIRECT	Sodium ion binding	3	1.30E-03	1.60E-02
KEGG_PATHWAY	cAMP signaling pathway	6	2.60E-03	2.00E-02
GOTERM_CC_DIRECT	Basolateral plasma membrane	5	3.00E-03	2.10E-02
KEGG_PATHWAY	Bile secretion	4	5.00E-03	3.40E-02
KEGG_PATHWAY	Cardiac muscle contraction	4	6.30E-03	4.00E-02
GOTERM_BP_DIRECT	Sodium ion transport	4	6.40E-03	1.20E-01
GOTERM_BP_DIRECT	Potassium ion transport	4	6.80E-03	1.20E-01
GOTERM_BP_DIRECT	Transport	13	7.60E-03	1.30E-01
KEGG_PATHWAY	cGMP-PKG signaling pathway	5	8.20E-03	4.90E-02
GOTERM_BP_DIRECT	Ion transport	7	8.40E-03	1.40E-01
KEGG_PATHWAY	Protein digestion and absorption	4	9.10E-03	5.10E-02
KEGG_PATHWAY	Pancreatic secretion	4	1.30E-02	6.50E-02
KEGG_PATHWAY	Thyroid hormone signaling pathway	4	1.80E-02	8.80E-02
GOTERM_MF_DIRECT	Chaperone binding	3	2.60E-02	2.00E-01
GOTERM_CC_DIRECT	Caveola	3	2.70E-02	1.20E-01
GOTERM_CC_DIRECT	Apical plasma membrane	3	2.50E-01	6.30E-01
GOTERM_MF_DIRECT	Hydrolase activity	7	4.00E-01	1.00E+00
GOTERM_MF_DIRECT	Metal ion binding	5	1.00E+00	1.00E+00
GOTERM_CC_DIRECT	Integral component of membrane	6	1.00E+00	1.00E+00
Annotation cluster 4—Enrichment score: 2.98				
GOTERM_MF_DIRECT	Cadherin binding involved in cell-cell adhesion	7	3.20E-04	6.50E-03
GOTERM_CC_DIRECT	Cell-cell adherens junction	7	3.30E-04	3.30E-03
GOTERM_MF_DIRECT	Unfolded protein binding	4	2.00E-03	2.20E-02
GOTERM_CC_DIRECT	Focal adhesion	6	5.90E-03	4.00E-02
Annotation cluster 5—Enrichment score: 2.37				
GOTERM_BP_DIRECT	ATP metabolic process	6	1.30E-07	2.00E-05
GOTERM_MF_DIRECT	ATPase activity	7	5.20E-05	1.40E-03
GOTERM_MF_DIRECT	Proton-transporting ATP synthase activity, rotational mechanism	3	9.60E-04	1.60E-02
GOTERM_CC_DIRECT	Mitochondrial proton-transporting ATP synthase complex	3	1.30E-03	9.30E-03
GOTERM_BP_DIRECT	ATP biosynthetic process	3	2.20E-03	5.20E-02

continued on next page

Category	Term	Count	P	Benjamini
GOTERM_BP_DIRECT	ATP synthesis–coupled proton transport	3	2.20E–03	5.20E–02
KEGG_PATHWAY	Huntington's disease	6	2.70E–03	2.00E–02
GOTERM_BP_DIRECT	Ion transport	7	8.40E–03	1.40E–01
KEGG_PATHWAY	Alzheimer's disease	5	1.10E–02	5.80E–02
GOTERM_BP_DIRECT	Proton transport	3	1.30E–02	2.10E–01
GOTERM_CC_DIRECT	Mitochondrial inner membrane	5	2.70E–02	1.20E–01
GOTERM_MF_DIRECT	Drug binding	3	5.40E–02	3.40E–01
KEGG_PATHWAY	Oxidative phosphorylation	3	1.50E–01	5.70E–01
KEGG_PATHWAY	Parkinson's disease	3	1.70E–01	5.80E–01
KEGG_PATHWAY	Metabolic pathways	7	6.10E–01	1.00E+00
Annotation cluster 6—Enrichment score: 2.29				
GOTERM_CC_DIRECT	Intracellular ribonucleoprotein complex	7	3.50E–04	3.30E–03
GOTERM_MF_DIRECT	Poly(A) RNA binding	11	3.40E–03	3.50E–02
GOTERM_MF_DIRECT	RNA binding	6	1.20E–01	6.10E–01
Annotation cluster 7—Enrichment score: 1.55				
GOTERM_CC_DIRECT	Melanosome	5	2.20E–04	2.30E–03
GOTERM_CC_DIRECT	Perinuclear region of cytoplasm	5	1.50E–01	4.10E–01
GOTERM_CC_DIRECT	Extracellular space	5	6.60E–01	1.00E+00
Annotation cluster 8—Enrichment score: 1.54				
GOTERM_CC_DIRECT	Intracellular ribonucleoprotein complex	7	3.50E–04	3.30E–03
GOTERM_BP_DIRECT	Translation	5	3.30E–02	3.90E–01
GOTERM_CC_DIRECT	Nucleolus	6	1.00E–01	3.00E–01
GOTERM_CC_DIRECT	Ribosome	3	1.10E–01	3.00E–01
KEGG_PATHWAY	Ribosome	3	1.60E–01	5.80E–01

be neuroprotective in models of brain ischemia (51, 52). Recent studies suggest that heat shock cognate 71 kDa, a cytosolic facilitator of protein folding and degradation, may have a strong interaction with Tau protein, a hallmark of AD (53). This protein has been suggested as a possible therapeutic target for stroke and TBI, as its overexpression may reduce apoptosis and inflammation (54).

Despite overlapping pathology, the connection between TBI and toxic mechanisms of neurodegenerative diseases, along with its potential therapeutic value, has yet to be fully elucidated (55). The unbiased identification of proteins involved in these processes acutely and subacutely in TBI through phage display further supports the notion that TBI initiates neurodegenerative signaling and provides prominent biomarkers for theragnostic applications.

While the current study successfully explores the utility of phage display–facilitated elucidation of TBI, there are limitations to the presented findings. First, the study implements a single unilateral CCI as the chosen TBI animal model, which does not recapitulate many other TBI phenotypes, such as repetitive mild head injury. However, no one animal model can fully recapitulate the human TBI experience (6). Therefore, it would be ideal to apply this phage display discovery pipeline to various animal models such as fluid percussion

injury and blast injury to compare and validate results. Second, the study finds no sex-dependent differences between injury groups, largely due to the intentional experimental design where phage elutions from male and female subjects were pooled together during biopanning. A future study increasing sample size and creating different biopanning pools for male and female brains would be a worthwhile endeavor, especially given recent findings of sex-dependent responses to neural inflammation and BBB disruption (33, 56). In addition, this biopanning process can be enhanced even further by assessing whether phages bind to peripheral cells that migrate to the injury site. This validation would be of special importance for potential studies that use *in vivo* phage display for shorter time points.

Another limitation of this described work is the stringency applied during the NGS discovery process. Sequences that showed binding to heart and spleen tissues were excluded in favor of sequences that bound only to injured brain tissue. In addition, sequences were selected for temporal specificity, excluding sequences that may have shown different enrichment profiles across the time points tested. The full dataset generated from this discovery pipeline may be used to identify more sequences that target different characteristics of neural injury.

The current study not only identified proteins specific to temporal TBI phases but also simultaneously developed targeting constructs for these candidate biomarkers. The design of HCDR3 constructs that specifically bind to acute and subacute brain injury provides a foundation for the development of theranostic tools. This discovery enables future characterization of the candidate targets through several conditions within the neural injury microenvironment, in addition to the refinement of HCDR3 constructs as a targeting modality to detect and treat TBI.

MATERIALS AND METHODS

CCI model

All experiments were approved by the Arizona State University Institutional Animal Care and Use Committee (IACUC) under protocols #17-1590R and #20-1793R. Eight-week-old male and female C57Bl/6 mice (Charles River) were assigned to four experimental groups: acute (1 dpi), subacute (7 dpi), chronic (21 dpi), and sham (craniotomy with no injury, sacrificed 1 day post-procedure). Mice were further divided for each experimental assay: biopanning [$n = 3$ mice biological replicates (mixed sex) per time point per biopanning round], IHC ($n = 3$ mice biological replicates per sex per time point), and IP-MS [$n = 3$ mice biological replicates (mixed sex) per time point]. For each experimental assay, mice were randomly distributed to a sacrifice time point while maintaining a mixed sex distribution for each subgroup. Briefly, mice were anesthetized with isoflurane (3% induction, 1.5% maintenance) and secured on a stereotaxic frame (Leica Microsystems, Wetzlar, Germany). A 3-mm craniotomy (–1 mm anteroposterior to bregma, 1.5 mm lateral to midline) was performed to accommodate a 2-mm-diameter, 1-mm-deep impact to the frontoparietal cortex at a velocity of 6 m/s and a duration of 100 ms. Surgical area was sutured, and then analgesics [buprenorphine (0.05 mg/kg)] and saline were subcutaneously administered. Mice were placed in single-housed cages and monitored during recovery.

In vivo biopanning

A human dAb library (Source Bioscience, Nottingham, UK) was prepared with hyperphage (Progen, Heidelberg, Germany) as described in the manufacturer's protocols (57). At 1, 7, or 21 dpi, the parent phage library (10^{12} to 10^{14} CFU in 100 μ l of saline) was administered via retro-orbital injection. Phage circulated for 10 min before animals were euthanized via pentobarbital solution overdose (150 mg/kg intraperitoneal injection). Nonspecific phages were cleared via thoracotomy and transcardial perfusion with 0.1 M phosphate buffer (pH 7.4). The ipsilateral (injured) and contralateral hemispheres of the brain were extracted and dissected, in addition to the peripheral organs—heart and spleen. Immediately, tissues were weighed, homogenized, pooled [$n = 3$ mice biological replicates (mixed sex) per biopanning round], and mechanically homogenized in chilled phosphate buffer with protease inhibitors. Trypsin was added to the homogenate to elute binding phage from tissue. Phage concentration determined by CFU of tissue elutions was quantified by bacteria titers (TG1 *Escherichia coli*). Titers were completed after each round to confirm distribution across tissues. Eluted phages were amplified with TG1 *E. coli* and stored under –80°C conditions. Between biopanning rounds, phage DNAs were isolated (QIAprep Spin Miniprep; Qiagen, Valencia, CA) and analyzed for sequence drift and/or convergence by the DNASU

Sequencing Core (Tempe, AZ). This procedure was repeated in sham animals.

For the second biopanning cycle, the eluted phages from the ipsilateral brain hemisphere were amplified and purified to serve as the phage population for the second biopanning round. Injection, tissue preparation, phage elution, amplification, and storage were completed as stated previously. A stock library from the manufacturer was amplified without a screening target to serve as a propagation library control to prevent selection of nonspecific, parasitic sequences.

NGS and analysis

Preparation of phage dAb libraries for deep sequencing was completed following the Illumina Nextera XT amplicon sequencing protocol (Illumina, San Diego, CA). Briefly, amplicons were created with a single polymerase chain reaction (PCR) step and Illumina-compatible indexes were added to each sample with a second PCR cycle. Phage libraries were sequenced with primers including Illumina-specific barcodes (table S6) via Illumina MiSeq 2 \times 300 bp (base pair) module by the DNASU Next Generation Sequencing Core at ASU Biodesign Institute (Tempe, AZ).

Paired-end sequences were stitched with fast length adjustment of short reads (FLASH) (58), using a minimum and maximum overlap of 10 and 200 bp, respectively. The HCDR3 sequence of each dAb was extracted in Bioconductor for R (59) by subsetting between dAb frameworks 3 and 4. Mutated HCDR3 sequences were excluded from analysis by filtering for sequence length. Raw RPMs were retrieved with the FASTAptamer Toolkit (60). HCDR3 sequences in injury groups that were determined to be enriched through biopanning (i.e., increase of reads from round 1 to round 2) were selected from each library. Enriched sequences were then compared with peripheral tissue (spleen and heart) and propagation control libraries to ensure final selection of HCDR3s that were specific to injured neural tissue libraries. Further, selected sequences were compared against other injury time points (i.e., sequences selected from acute injury were compared with sequences from the subacute injury group) using z scores to enhance temporal specificity for each sequence selection. Top HCDR3s were selected for antibody-mimetic production and further validation based on the following criteria: (i) frequency, (ii) fold enrichment values, and (iii) specificity to neural injury at the distinct biopanning time points.

Biotinylated HCDR3 constructs

HCDR3 peptides for injury and control groups were synthesized with N- and C-terminal Cys for preparation of constrained peptide constructs (WatsonBio, Houston, TX). Peptides were then conjugated to a bivalent peptide linker (61) that used thiol-bromoacetamide conjugation to constrain the peptides via the N- and C-terminal Cys (custom order from Sigma-Aldrich, St. Louis, MO). The peptide linker contained a C-terminal biotin. Each reaction was analyzed by MALDI to confirm the presence of the peptide-scaffold conjugate (fig. S5). Constructs were purified via HPLC collection at 214 nm for downstream analyses.

Immunohistochemistry

Mice were subjected to CCI or sham ($n = 3$ biological replicates per sex per time point) as described previously and perfused with 0.1 M phosphate buffer and 4% paraformaldehyde at designated time points. Brains were fixed overnight in 4% paraformaldehyde at 4°C, followed by immersion in 15% sucrose and then 30% sucrose. Brains

were flash-frozen on dry ice in optimal cutting temperature medium and stored at -80°C . Samples were sectioned coronally at $20\ \mu\text{m}$ thickness. After incubation with excess streptavidin and biotin to block endogenous biotin (Endogenous Biotin Blocking Kit; Thermo Fisher Scientific, Waltham, MA), $5\ \mu\text{M}$ biotinylated HCDR3 construct was incubated on tissue overnight at 4°C . Simultaneously, control sections were incubated with control HCDR3 construct or $1\times$ phosphate-buffered saline (PBS). Tissue sections were washed in $1\times$ PBS, and then HCDR3 construct samples were incubated with Alexa Fluor 555 streptavidin (1:1000; Invitrogen, catalog no. S21381) at room temperature for 2 hours, followed by three $1\times$ PBS washes. Tissue sections were subjected to 4',6-diamidino-2-phenylindole (DAPI) incubation for 5 min. Three sections per mouse were visualized using fluorescence microscopy, and $20\times$ magnification tile scans were prepared for processing using ImageJ software. Threshold values of control slices were used to quantify fraction of HCDR3 construct positive staining. Analyzed area was approximately $1500\ \mu\text{m} \times 1500\ \mu\text{m}$. Analysis was conducted while blind to injury condition. Sample size was determined via power analysis of prior IHC data variability in the laboratory.

Immunoprecipitation–mass spectrometry

CCI and sham surgeries were completed as described previously [$n = 3$ biological replicates (mixed sex) per time point]. Mice were sacrificed at 1 or 7 dpi via transcardial perfusion with phosphate buffer (pH 7.4). The ipsilateral hemisphere of the brain was immediately dissected and homogenized in chilled lysis buffer ($1\times$ PBS, 1% Triton X-100, protease inhibitor cocktail). Protein concentration was quantified with the Pierce BCA Protein Assay Kit (Thermo Fisher Scientific).

Streptavidin-coupled Dynabeads (Thermo Fisher Scientific) were washed with 0.1% Tween 20 in $1\times$ PBS and incubated with tissue lysate (1 mg/ml) for 1 hour at room temperature. Precleared lysate was collected after separation from magnetic beads and incubated with designated HCDR3 constructs rotating overnight at 4°C to form the immune complex. The immune complex was incubated with streptavidin-coupled Dynabeads for 1 hour at room temperature, and beads were then washed three times with chilled lysis buffer. Antigens were eluted directly from beads with 0.2% Rapigest for LC-MS analysis using the Thermo Orbitrap Fusion Lumos (Thermo Fisher Scientific) by the ASU Biodesign Mass Spectrometry Facility. Three biological replicates (mixed sex) per HCDR3 construct were sent for analysis to ensure stringency. Functional annotation clustering of proteins was conducted with DAVID to identify significant gene ontology terms represented in LC-MS data (62). Analysis was restricted to proteins identified in more than one biological replicate sample.

Statistics

For NGS analysis, raw counts were first normalized to RPMs to account for library differences. A normalized z score was then used as a threshold to identify HCDR3s that were highly represented and specific to their distinct injury time point. Selected HCDR3s were then screened for enrichment factor and individual frequency. For IHC, fluorescence percentage per area was conducted with ordinary one-way analysis of variance (ANOVA) followed by Tukey's post hoc test for multiple comparisons; statistical significance was determined as $P < 0.05$. For IP-MS, identified proteins that met the FDR threshold of <0.01 were used in all ontological assessments to categorize biological processes and candidate pathways.

SUPPLEMENTARY MATERIALS

Supplementary material for this article is available at <https://science.org/doi/10.1126/sciadv.abo5047>

[View/request a protocol for this paper from Bio-protocol.](#)

REFERENCES AND NOTES

- M. Faul, L. Xu, M. M. Wald, V. G. Coronado, *Traumatic Brain Injury in the United States* (Centers for Disease Control and Prevention, National Center for Injury Prevention Control, 2010).
- T. A. Ashman, J. B. Cantor, W. A. Gordon, A. Sacks, L. Spielman, M. Egan, M. R. Hibbard, A comparison of cognitive functioning in older adults with and without traumatic brain injury. *J. Head Trauma Rehabil.* **23**, 139–148 (2008).
- T. M. Sivanandam, M. K. Thakur, Traumatic brain injury: A risk factor for Alzheimer's disease. *Neurosci. Biobehav. Rev.* **36**, 1376–1381 (2012).
- S. A. Acosta, N. Tajiri, I. de la Pena, M. Bastawrous, P. R. Sanberg, Y. Kaneko, C. V. Borlongan, Alpha-synuclein as a pathological link between chronic traumatic brain injury and Parkinson's disease. *J. Cell. Physiol.* **230**, 1024–1032 (2015).
- Centers for Disease Control and Prevention (CDC), CDC grand rounds: Reducing severe traumatic brain injury in the United States. *MMWR Morb. Mortal. Wkly. Rep.* **62**, 549–552 (2013).
- Y. Xiong, A. Mahmood, M. Chopp, Animal models of traumatic brain injury. *Nat. Rev. Neurosci.* **14**, 128–142 (2013).
- Y. Xiong, A. Mahmood, M. Chopp, Emerging treatments for traumatic brain injury. *Expert Opin. Emerg. Drugs* **14**, 67–84 (2009).
- E. Czeiter, K. Amrein, B. Y. Gravesteyn, F. Lecky, D. K. Menon, S. Mondello, V. F. J. Newcombe, S. Richter, E. W. Steyerberg, T. Vande Vyvere, J. Verheyden, H. Xu, Z. Yang, A. I. R. Maas, K. K. W. Wang, A. Büki; CENTER-TBI Participants and Investigators, Blood biomarkers on admission in acute traumatic brain injury: Relations to severity, CT findings and care path in the CENTER-TBI study. *EBioMedicine* **56**, 102785 (2020).
- P. K. Dash, J. Zhao, G. Hergenroeder, A. N. Moore, Biomarkers for the diagnosis, prognosis, and evaluation of treatment efficacy for traumatic brain injury. *Neurotherapeutics* **7**, 100–114 (2010).
- W. T. O'Brien, L. Pham, G. F. Symons, M. Monif, S. R. Shultz, S. J. McDonald, The NLRP3 inflammasome in traumatic brain injury: Potential as a biomarker and therapeutic target. *J. Neuroinflammation* **17**, 104 (2020).
- S. Kumar, Z. Fritz, K. Sulakhiya, T. Theis, F. Berthiaume, Transcriptional factors and protein biomarkers as target therapeutics in traumatic spinal cord and brain injury. *Curr. Neuropharmacol.* **18**, 1092–1105 (2020).
- F. H. Kobeissy, J. D. Guingab-Cagmat, Z. Zhang, A. Moghieb, O. Y. Glushakova, S. Mondello, A. M. Boutté, J. Anagli, R. Rubenstein, H. Bahmad, A. K. Wagner, R. L. Hayes, K. K. W. Wang, Neuroproteomics and systems biology approach to identify temporal biomarker changes post experimental traumatic brain injury in rats. *Front. Neurol.* **7**, 198 (2016).
- A. K. Ottens, F. H. Kobeissy, E. C. Golden, Z. Zhang, W. E. Haskins, S. S. Chen, R. L. Hayes, K. K. W. Wang, N. D. Denslow, Neuroproteomics in neurotrauma. *Mass Spectrom. Rev.* **25**, 380–408 (2006).
- J. D. Guingab-Cagmat, K. Newsom, A. Vakulenko, E. B. Cagmat, F. H. Kobeissy, S. Zoltewicz, K. K. Wang, J. Anagli, In vitro MS-based proteomic analysis and absolute quantification of neuronal-glial injury biomarkers in cell culture system. *Electrophoresis* **33**, 3786–3797 (2012).
- C. Ma, G. Yin, D. Yan, X. He, L. Zhang, Y. Wei, Z. Huang, A novel peptide specifically targeting ovarian cancer identified by in vivo phage display. *J. Pept. Sci.* **19**, 730–736 (2013).
- J. Bábíčková, L. Tóthová, P. Boor, P. Celec, In vivo phage display—A discovery tool in molecular biomedicine. *Biotechnol. Adv.* **31**, 1247–1259 (2013).
- A. P. Mann, P. Scodeller, S. Hussain, J. Joo, E. Kwon, B. Gary, A peptide for targeted, systemic delivery of imaging and therapeutic compounds into acute brain injuries. *Nat. Commun.* **7**, 11980 (2016).
- S. Ghoshal, V. Bondada, K. E. Saatman, R. P. Guttmann, J. W. Geddes, Phage display for identification of serum biomarkers of traumatic brain injury. *J. Neurosci. Methods* **272**, 33–37 (2016).
- D. Christ, K. Famm, G. Winter, Repertoires of aggregation-resistant human antibody domains. *Protein Eng. Des. Sel.* **20**, 413–416 (2007).
- A. Bates, C. A. Power, David vs. Goliath: The structure, function, and clinical prospects of antibody fragments. *Antibodies* **8**, 28 (2019).
- Y. J. Deng, A. L. Notkins, Molecular determinants of polyreactive antibody binding: HCDR3 and cyclic peptides. *Clin. Exp. Immunol.* **119**, 69–76 (2000).
- D. Frenkel, B. Solomon, Filamentous phage as vector-mediated antibody delivery to the brain. *Proc. Natl. Acad. Sci.* **99**, 5675–5679 (2002).
- A. Muruganandam, J. Tanha, S. Narang, D. Stanimirovic, Selection of phage-displayed llama single-domain antibodies that transigrate across human blood-brain barrier endothelium. *FASEB J.* **16**, 240–242 (2002).

24. E. Sasso, R. Paciello, F. D'Auria, G. Riccio, G. Froehlich, R. Cortese, A. Nicosia, C. De Lorenzo, N. Zambrano, One-step recovery of scFv clones from high-throughput sequencing-based screening of phage display libraries challenged to cells expressing native claudin-1. *Biomed. Res. Int.* **2015**, 1–9 (2015).
25. S. Lykkemark, O. A. Mandrup, N. A. Friis, P. Kristensen, Degradation of C-terminal tag sequences on domain antibodies purified from *E. coli* supernatant. *MABS* **6**, 1551–1559 (2014).
26. G.-H. Yan, K. Wang, Z. Shao, L. Luo, Z.-M. Song, J. Chen, R. Jin, X. Deng, H. Wang, Z. Cao, Y. Liu, A. Cao, Artificial antibody created by conformational reconstruction of the complementary-determining region on gold nanoparticles. *Proc. Natl. Acad. Sci. U.S.A.* **115**, E34–E43 (2017).
27. C. Monnet, D. Laune, J. Laroche-Traineau, M. Biard-Piechaczyk, L. Briant, C. Bès, M. Pugnère, J. C. Mani, B. Pau, M. Cerutti, G. Devauchelle, C. Devaux, C. Granier, T. Chardès, Synthetic peptides derived from the variable regions of an anti-CD4 monoclonal antibody bind to CD4 and inhibit HIV-1 promoter activation in virus-infected cells. *J. Biol. Chem.* **274**, 3789–3796 (1999).
28. J. Chung, C. Rader, M. Popkov, Y.-M. Hur, H.-K. Kim, Y.-J. Lee, C. F. Barbas III, Integrin $\alpha_{IIb}\beta_3$ -specific synthetic human monoclonal antibodies and HCDR3 peptides that potentially inhibit platelet aggregation. *FASEB J.* **18**, 361–363 (2004).
29. Y. Barrios, P. Jirholt, M. Ohlin, Length of the antibody heavy chain complementarity determining region 3 as a specificity-determining factor. *J. Mol. Recognit.* **17**, 332–338 (2004).
30. L. J. Holt, C. Herring, L. S. Jespers, B. P. Woolven, I. M. Tomlinson, Domain antibodies: Proteins for therapy. *Trends Biotechnol.* **21**, 484–490 (2003).
31. A. P. Mann, P. Scodeller, S. Hussain, G. B. Braun, T. Mölder, K. Toome, R. Ambasadhan, T. Teesalu, S. A. Lipton, E. Ruoslahti, Identification of a peptide recognizing cerebrovascular changes in mouse models of Alzheimer's disease. *Nat. Commun.* **8**, 1403 (2017).
32. S. A. Baldwin, I. Fugaccia, D. R. Brown, L. V. Brown, S. W. Scheff, Blood-brain barrier breach following cortical contusion in the rat. *J. Neurosurg.* **85**, 476–481 (1996).
33. V. N. Bharadwaj, C. Copeland, E. Mathew, J. Newbern, T. R. Anderson, J. Lifshitz, V. D. Kodibagkar, S. E. Stabenfeldt, Sex-dependent macromolecule and nanoparticle delivery in experimental brain injury. *Tissue Eng. Part A* **26**, 688–701 (2020).
34. G. W. Liu, B. R. Livesay, N. A. Kacherovsky, M. Cieslewicz, E. Lutz, A. Waalkes, M. C. Jensen, S. J. Salpante, S. H. Pun, Efficient identification of murine M2 macrophage peptide targeting ligands by phage display and next-generation sequencing. *Bioconjug. Chem.* **26**, 1811–1817 (2015).
35. P. A. C. t Hoen, S. M. G. Jirka, B. R. Ten Broeke, E. A. Schultes, B. Aguilera, K. H. Pang, H. Heemskerck, A. Aartsma-Rus, G. J. Van Ommen, J. T. Den Dunnen, Phage display screening without repetitive selection rounds. *Anal. Biochem.* **421**, 622–631 (2012).
36. M. Takahashi, A. Ueno, H. Mihara, Peptide design based on an antibody complementarity-determining region (CDR): Construction of porphyrin-binding peptides and their affinity maturation by a combinatorial method. *Chemistry* **6**, 3196–3203 (2000).
37. S. Mulherkar, K. F. Tolias, RhoA-ROCK signaling as a therapeutic target in traumatic brain injury. *Cell* **9**, 245 (2020).
38. T. R. Stankiewicz, D. A. Linseman, Rho family GTPases: Key players in neuronal development, neuronal survival, and neurodegeneration. *Front. Cell. Neurosci.* **8**, 314 (2014).
39. M. Chen, H. Song, J. Cui, C. E. Johnson, G. K. Hubler, R. G. Depalma, Z. Gu, W. Xia, Proteomic profiling of mouse brains exposed to blast-induced mild traumatic brain injury reveals changes in axonal proteins and phosphorylated tau. *J. Alzheimers Dis.* **66**, 751–773 (2018).
40. C. K. Franz, D. Joshi, E. L. Daley, R. A. Grant, K. Dalamatgas, A. Leung, J. D. Finan, E. Kiskinis, Impact of traumatic brain injury on amyotrophic lateral sclerosis: From bedside to bench. *J. Neurophysiol.* **122**, 1174–1185 (2019).
41. V. Delic, K. D. Beck, K. C. H. Pang, B. A. Citron, Biological links between traumatic brain injury and Parkinson's disease. *Acta Neuropathol. Commun.* **8**, 45 (2020).
42. G. Edwards III, I. Moreno-Gonzalez, C. Soto, Amyloid-beta and tau pathology following repetitive mild traumatic brain injury. *Biochem. Biophys. Res. Commun.* **483**, 1137–1142 (2017).
43. D. Tian, R. I. Dmitrieva, P. A. Doris, J. F. Crary, R. Sondhi, T. C. Sacktor, P. J. Bergold, Protein kinase M zeta regulation of Na/K ATPase: A persistent neuroprotective mechanism of ischemic preconditioning in hippocampal slice cultures. *Brain Res.* **1213**, 127–139 (2008).
44. C. M. Atkins, S. Chen, O. F. Alonso, W. D. Dietrich, B. R. Hu, Activation of calcium/calmodulin-dependent protein kinases after traumatic brain injury. *J. Cereb. Blood Flow Metab.* **26**, 1507–1518 (2006).
45. Q. Lu, V. A. Harris, X. Sun, Y. Hou, S. M. Black, Ca^{2+} /calmodulin-dependent protein kinase II contributes to hypoxic ischemic cell death in neonatal hippocampal slice cultures. *PLOS ONE* **8**, e70750 (2013).
46. A. B. Enogieru, S. I. Omoruyi, D. C. Hiss, O. E. Ekpo, GRP78/BIP/HSPA5 as a therapeutic target in models of Parkinson's disease: A mini review. *Adv. Pharmacol. Sci.* **2019**, 1–11 (2019).
47. E. Colla, Linking the endoplasmic reticulum to Parkinson's disease and alpha-synucleinopathy. *Front. Neurosci.* **13**, 560 (2019).
48. J. J. M. Hoozemans, R. Veerhuis, E. S. Van Haastert, J. M. Rozemuller, F. Baas, P. Eikelenboom, W. Scheper, The unfolded protein response is activated in Alzheimer's disease. *Acta Neuropathol.* **110**, 165–172 (2005).
49. A. S. Lee, The ER chaperone and signaling regulator GRP78/BIP as a monitor of endoplasmic reticulum stress. *Methods* **35**, 373–381 (2005).
50. K.-W. Park, G. E. Kim, R. Morales, F. Moda, I. Moreno-Gonzalez, L. Concha-Marambio, A. S. Lee, C. Hetz, C. Soto, The endoplasmic reticulum chaperone GRP78/BIP modulates prion propagation in vitro and in vivo. *Sci. Rep.* **7**, 44723 (2017).
51. T. Kudo, S. Kanemoto, H. Hara, N. Morimoto, T. Morihara, R. Kimura, T. Tabira, K. Imaizumi, M. Takeda, A molecular chaperone inducer protects neurons from ER stress. *Cell Death Differ.* **15**, 364–375 (2008).
52. Y. Oida, H. Izuta, A. Oyagi, M. Shimazawa, T. Kudo, K. Imaizumi, H. Hara, Induction of BIP, an ER-resident protein, prevents the neuronal death induced by transient forebrain ischemia in gerbil. *Brain Res.* **1208**, 217–224 (2008).
53. I. R. Taylor, A. Ahmad, T. Wu, B. A. Nordhues, A. Bhullar, J. E. Gestwicki, E. R. P. Zuiderweg, The disorderly conduct of Hsc70 and its interaction with the Alzheimer's-related Tau protein. *J. Biol. Chem.* **293**, 10796–10809 (2018).
54. R. G. Giffard, L. Xu, H. Zhao, W. Carrico, Y. Ouyang, Y. Qiao, R. Sapolsky, G. Steinberg, B. Hu, M. A. Yenari, Chaperones, protein aggregation, and brain protection from hypoxic/ischemic injury. *J. Exp. Biol.* **207**, 3213–3220 (2004).
55. J. Ramos-Cejudo, T. Wisniewski, C. Marmar, H. Zetterberg, K. Blennow, M. J. de Leon, S. Fossati, Traumatic brain injury and Alzheimer's disease: The cerebrovascular link. *EBioMedicine* **28**, 21–30 (2018).
56. S. Villapol, D. J. Loane, M. P. Burns, Sexual dimorphism in the inflammatory response to traumatic brain injury. *Glia* **65**, 1423–1438 (2017).
57. C. M. Y. Lee, N. Iorno, F. Siero, D. Christ, Selection of human antibody fragments by phage display. *Nat. Protoc.* **2**, 3001–3008 (2007).
58. T. Magoč, S. L. Salzberg, FLASH: Fast length adjustment of short reads to improve genome assemblies. *Bioinformatics* **27**, 2957–2963 (2011).
59. R. C. Gentleman, V. J. Carey, D. M. Bates, B. Bolstad, M. Dettling, S. Dudoit, B. Ellis, L. Gautier, Y. Ge, J. Gentry, K. Hornik, T. Hothorn, W. Huber, S. Iacus, R. Irizarry, F. Leisch, C. Li, M. Maechler, A. J. Rossini, G. Sawitzki, C. Smith, G. Smyth, L. Tierney, J. Y. H. Yang, J. Zhang, Bioconductor: Open software development for computational biology and bioinformatics. *Genome Biol.* **5**, R80 (2004).
60. K. K. Alam, J. L. Chang, D. H. Burke, FASTAptamer: A bioinformatic toolkit for high-throughput sequence analysis of combinatorial selections. *Mol. Ther. Acids* **4**, e230 (2015).
61. J. C. Lainson, M. F. Fuenmayor, S. A. Johnston, C. W. Diehnelt, Conjugation approach to produce a *Staphylococcus aureus* synbody with activity in serum. *Bioconjug. Chem.* **26**, 2125–2132 (2015).
62. G. Dennis, B. T. Sherman, D. A. Hosack, J. Yang, W. Gao, H. C. Lane, R. A. Lempicki, DAVID: Database for annotation, visualization, and integrated discovery. *Genome Biol.* **4**, P3 (2003).

Acknowledgments: We acknowledge the following facilities and/or personnel for support: ASU Genomics Facility and S. Yang for NGS support, ASU Mass Spectrometry Core and T. Karr for MS services, A. Witten for figure illustrations, and N. Borgogni for IHC assistance. **Funding:** This work was supported by NIH NICHD 1DP2HD084067 (S.E.S.), NIH NICHD 1DP2HD084067-01S1 (S.E.S.), NIH NINDS 1R21NS107985 (S.E.S.), ARCS Scholar Award (B.I.M.), and ASU Biomimicry Seed funding (C.W.D., N.S., and S.E.S.). **Author contributions:** Conceptualization: B.I.M. and S.E.S. Methodology: B.I.M., S.E.S., C.W.D., and N.S. Experimentation: B.I.M., G.A.M., K.F., and T.M. Supervision: S.E.S., C.W.D., and N.S. Writing—original draft: B.I.M. and S.E.S. Writing—review and editing: B.I.M., S.E.S., C.W.D., and N.S. **Competing interests:** B.I.M., S.E.S., C.W.D., and N.S. are inventors on a patent application related to this work filed by ASU (11157.047PCT, filed on 20 June 2020). The authors declare no other competing interests. **Data and materials availability:** All data needed to evaluate the conclusions in the paper are present in the paper and/or the Supplementary Materials. All materials and supplies were commercially available with the exception of the custom-designed peptide systems whereby the methods describe fabrication and production using standard biochemistry approaches. All datasets for the phage NGS and IP-MS experiments are available at ASU Dataverse: Martinez, Briana; Stabenfeldt, Sarah, 2022, "Replication data for: Uncovering temporospatial sensitive TBI targeting strategies via in vivo phage display," <https://doi.org/10.48349/ASU/ZTW1HN>, ASU Library Research Data Repository, V1, UNF:6sK235WMT38kbnxmkR4w0g== [fileUNF].

Submitted 7 February 2022

Accepted 28 May 2022

Published 22 July 2022

10.1126/sciadv.abo5047